Published in "Physical Review B 87(16): 165139, 2013"
which should be cited to refer to this work.

Non-Fermi-liquid behavior in cubic phase $BaRuO_3$: A dynamical mean-field study

Li Huang[1,2,3] and Bingyun Ao[1]

[1]*Science and Technology on Surface Physics and Chemistry Laboratory, P.O. Box 718-35, Mianyang 621907, Sichuan, China*
[2]*Beijing National Laboratory for Condensed Matter Physics, and Institute of Physics, Chinese Academy of Sciences, Beijing 100190, China*
[3]*Department of Physics, University of Fribourg, Fribourg CH-1700, Switzerland*

Motivated by the recently synthesized cubic phase $BaRuO_3$ under high pressure and high temperature, a thorough study has been conducted on its temperature-dependent electronic properties by using the state-of-the-art *ab initio* computing framework of density-functional theory combined with dynamical mean-field theory. At ambient condition the cubic phase $BaRuO_3$ should be a correlated Hund's metal with frozen spin magnetic moment. The spin-spin correlation function and local magnetic susceptibility can be well described by the Curie-Weiss law over a wide temperature range. The calculated low-frequency self-energy functions of Ru $4d$ states apparently deviate from the behaviors predicted by Landau Fermi-liquid theory. Beyond that, the low-frequency optical conductivity can be fitted to a power law $\Re\sigma(\omega) \sim \omega^{-0.98}$, which further confirms the non-Fermi-liquid metallic state.

I. INTRODUCTION

Recently the alkaline-earth ruthenium oxides have attracted growing interest. These oxides generally exhibit fascinating physics properties, such as unconventional superconductivity with p-wave symmetry (Sr_2RuO_4),[1] antiferromagnetic Mott insulator (Ca_2RuO_4) (Ref. 2), and orbital selective Mott transition ($Sr_{2-x}Ca_xRuO_4$),[3] etc. Among the rest, due to their interesting magnetic phase diagrams, transport properties, and potential device applications, the ternary ruthenates with perovskite or perovskite-related structures ($MRuO_3$: M = Ca, Sr, Ba) have been extensively studied by numerous experiments and theoretical calculations in the past decade.[4–17]

Both $CaRuO_3$ and $SrRuO_3$ crystallize in the orthorhombic perovskite structure with a $GdFeO_3$-type distortion. $SrRuO_3$ is a highly correlated, narrow-band metallic ferromagnet with Curie temperature (T_c) of about 160 K.[4] Its local magnetic moment (1.4 μ_B) is rather large, despite the highly extended $4d$ character of the valence electrons. Interestingly, $CaRuO_3$, an isostructural compound, does not show any magnetic ordering at finite temperatures.[5] The nature of its magnetic ground state still remains controversial. We note that one of the most striking properties of $CaRuO_3$ and $SrRuO_3$ compounds is the violation of Landau Fermi-liquid (LFL) theory, which has been proven by many experimental results, including x-ray photoemission spectra, transport and optical properties, etc.[6–9] The strength of Coulomb interaction U and the importance of Hund's rule coupling J among Ru-$4d$ orbitals are two other interesting topics in lively debate. Though almost all of the experimental[10–12] and theoretical[13–15] efforts manifest some roles of electron-electron correlation, the strength and the extent of its importance still remains unclear.

In the earlier years, it was well known that depending on how $BaRuO_3$ is synthesized it has several polytype structures, i.e., the nine-layered rhombohedral (9R), the four-layered hexagonal (4H), and the six-layered hexagonal (6H).[16,17] Lately, the cubic phase $BaRuO_3$ with ideal perovskite structure has been synthesized by Jin *et al*. under 18 GPa at 1000 °C.[18] It remains metallic down to 4 K and a ferromagnetic transition occurs at $T_c = 60$ K,[19] which is significantly lower than that of $SrRuO_3$.[4] The ferromagnetic transition in $SrRuO_3$ falls into the mean-field universality class, whereas cubic phase $BaRuO_3$ exhibits significant critical fluctuations as described by the three-dimensional (3D) Heisenberg model.[19] The availability of perovskite-structure $BaRuO_3$ not only completes its polymorph, but also makes it possible to map out the evolution of magnetism, correlation strength, and other properties as a function of the ionic size of the M site in the whole series of $MRuO_3$.[18]

Despite the fact that tremendous efforts have been made, little is known about the basic properties of cubic phase $BaRuO_3$. In this paper, we will mainly address the following two issues: (i) Definitely, in $CaRuO_3$ and $SrRuO_3$, the effects induced by electronic correlation cannot be ignored.[10–15] However, does the electronic correlation play a decisive role in cubic phase $BaRuO_3$? (ii) It is believed that the physical properties of $CaRuO_3$ and $SrRuO_3$ at ambient condition cannot be well described by the LFL theory. Indeed, the key evidences are their low-frequency optic conductivity, resistivity, and electronic Raman scattering intensity which obey the fractional power law.[6–9] Thus, whether the physical properties of cubic phase $BaRuO_3$ still violate the LFL theory becomes an essential and interesting problem.

The density-functional theory within local density approximation combined with dynamical mean-field theory (dubbed LDA + DMFT) is a very powerful computing framework for strongly correlated materials.[20–22] In the present works, by employing the LDA + DMFT computational scheme, the temperature-dependent electronic properties of cubic phase $BaRuO_3$ have been systematically studied. In contrast to $CaRuO_3$ and $SrRuO_3$, under room temperature the cubic phase $BaRuO_3$ is a moderately correlated Hund's metal with frozen spin magnetic moment, and its low-frequency conductivity obviously deviates the ω^{-2} law, as is predicted by classic Fermi-liquid theory.

II. METHOD

We first compute the ground-state electronic structures of cubic phase $BaRuO_3$ within nonmagnetic configuration by utilizing the plane-wave pseudopotential approach as is

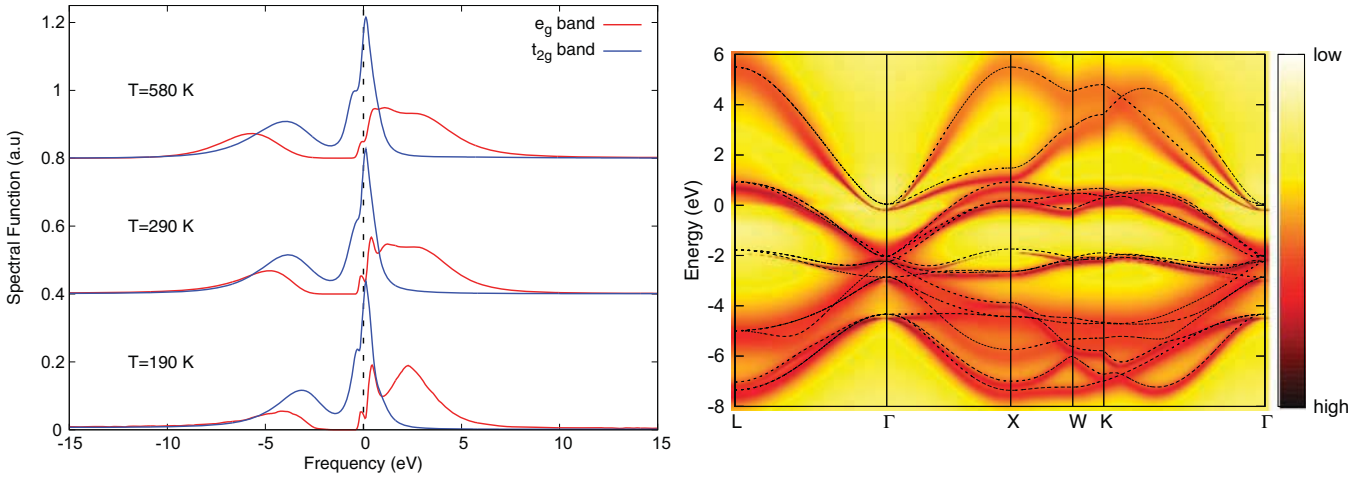

FIG. 1. (Color online) Spectral functions of cubic perovskite $BaRuO_3$ calculated by LDA + DMFT method. Left panel: Spectral functions of Ru $4d$ states at various temperatures. Right panel: Quasiparticle band structure of $BaRuO_3$ along high-symmetry lines in the Brillouin zone. The dashed lines denote corresponding LDA band structure.

implemented in the QUANTUM ESPRESSO software package.[23] The generalized gradient approximation with Perdew-Burke-Ernzerhof exchange-correlation functional[24] is used to describe the exchange and correlation potentials. The pseudopotentials in a projector augmented wave scheme[25] for Ba, Ru, and O species were built by us. The electronic wave functions are described with a plane-wave basis truncated at 80 Ha, and a Γ-centered $12 \times 12 \times 12$ k-point grid for Brillouin zone integrations is adopted. These pseudopotentials and computational parameters are carefully checked and tuned to ensure the numerical convergences.

To include the effect of electronic correlations, the ground-state wave functions are used to construct a basis of maximally localized Wannier functions (MLWF) for Ru $4d$ and O $2p$ orbitals. The corresponding multiband Hubbard Hamiltonian has the following form:[21,22]

$$H_{\mathrm{LDA+DMFT}} = H_{\mathrm{LDA}} - H_{\mathrm{DC}} + \sum_{imm'} \frac{U_{mm'}}{2} n_{im} n_{im'}, \qquad (1)$$

where $n_{im} = c^{\dagger}_{im} c_{im}$, and $c^{\dagger}_{im}(c_{im})$ creates (destroys) an electron in a Wannier orbital m at site i. Here H_{LDA} is the effective low-energy Hamiltonian in the basis of Ru $4d$ and O $2p$ MLWF orbitals and thus is a 14×14 matrix. H_{DC} is a double-counting correction term which accounts for the electronic correlation already described by the LDA part, and the fully local limit scheme[26] is chosen. The Coulomb interaction is taken into consideration merely among the Ru $4d$ orbitals. We use $U = 4.0$ eV and $J = 0.65$ eV to parametrize the Coulomb interaction matrix, which are close to previous estimations.[14,15] To solve the many-body Hamiltonian (1), in the DMFT part[20,21] we employ the hybridization expansion continuous-time quantum Monte Carlo impurity solver (abbreviated CT-HYB).[27,28] The Legendre orthogonal polynomial representation[29] and improved estimator for the self-energy function[30] are implemented into our CT-HYB quantum impurity solver to improve the numerical accuracy. Finally, through the mature analytical continuation methods[31,32] the impurity spectral functions can be extracted directly from the imaginary-time Green's functions which are derived from the quantum Monte Carlo simulations. Additionally, the impurity self-energy functions on a real axis are obtained by using the trick proposed by Haule *et al.*[33]

III. RESULTS AND DISCUSSION

Figure 1 (see upper panel) represents our calculated orbital-resolved density of states for Ru $4d$ states at several typical temperatures. The octahedral surrounding of Ru splits the Ru $4d$ states into threefold-degenerated t_{2g} and twofold-degenerated e_g levels. Ru^{4+} ion, which is nominally in a low-spin d^4 configuration, gives rise to a t^4_{2g} configuration with Fermi level lying in the t_{2g} manifold with empty e_g states. As for the density of states of t_{2g} states, it displays a sharp quasiparticle peak near the Fermi level, a shoulder structure around -0.3 eV, and a Hubbard subbandlike hump at -8.0 eV ~ -2.0 eV. While for the density of states of e_g states, since it is less occupied, the primary spectral weight is above the Fermi level. There are two small satellites located on both sides of the Fermi level (-0.1 and 0.3 eV, respectively). With the increment of temperature, the two peaks will be smeared out gradually. To sum up, the integrated spectral functions of Ru $4d$ states show significantly metallic features, and the temperature effect is not very obvious. When the temperature rises from 190 to 580 K, slightly spectral weight transfer to high energy is observed. In the integrated spectral functions of Ru $4d$ states, quite-well-developed Hubbard bands are founded. We note that in the previous LDA + DMFT calculations for $SrRuO_3$ and $CaRuO_3$,[14] similar features in their integrated spectral functions are observed too. This might be due to the downfolding procedure within which all the hybridizations between the Ru $4d$ and O $2p$ states are not completely taken into account, and the one-shot LDA + DMFT computational scheme in which the charge density is not fully self-consistent.[34]

In the next step, we computed the fully momentum-resolved spectral function $A(\vec{k},\omega)$ along some high-symmetry lines in the Brillouin zone for cubic phase $BaRuO_3$. The inverse

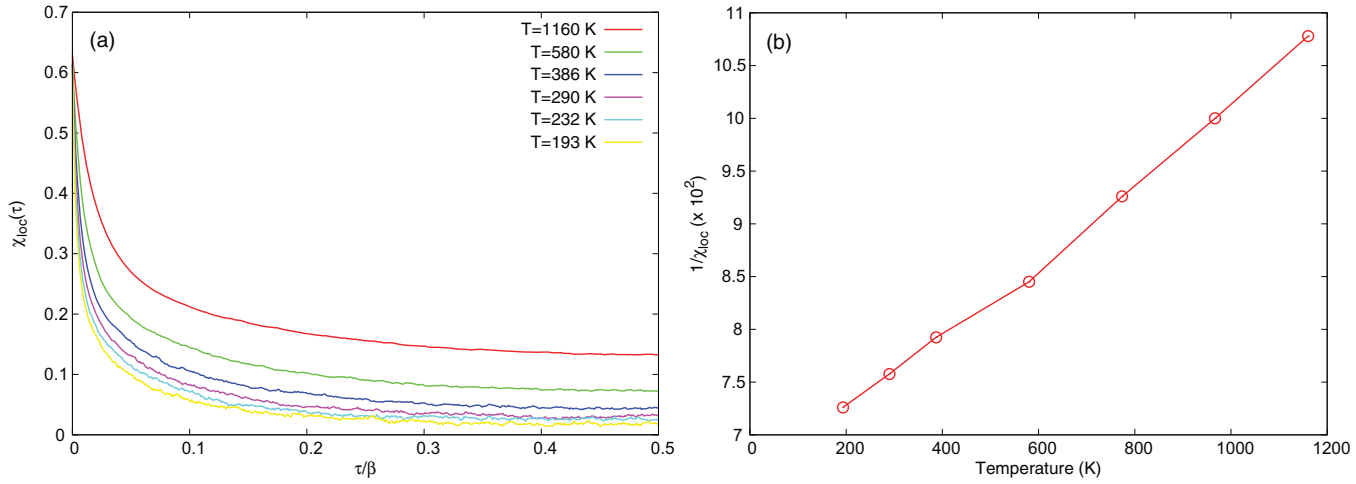

FIG. 2. (Color online) Magnetic properties of cubic perovskite $BaRuO_3$. (a) Spin-spin correlation functions $\chi(\tau) = \langle S_z(0)S_z(\tau)\rangle$ at various temperatures. (b) Inverse local magnetic susceptibility $\chi_{\rm loc}^{-1}$ as a function of temperature.

temperature β is chosen to be 40, which corresponds to $T = 290$ K approximately. In the lower panel of Fig. 1, $A(\vec{k},\omega)$ is shown in comparison with the LDA band structure. The sharp quasiparticle peak observed in the integrated spectral function is clearly visible on the intensity plot and fairly well defined. It lies in the region from about -2.0 eV to 1.5 eV, dominated by the t_{2g} states. At higher energy, the e_g states become the majority. However, in the region below -2.0 eV, the O $2p$ states make a major contribution. From the distributions of spectral weights of t_{2g} and e_g states, it is speculated that in the region from -2.0 to -7.0 eV, there exists strong hybridization between the Ru $4d$ and O $2p$ states. Comparing this with the LDA band structure, first of all we notice that the quasiparticle band structure does not show apparent shifting. Secondly, except for becoming diffuse, the band renormalization of the quasiparticle band structure is hard to be distinguished, which means small effective masses. Note that from 190 to 1160 K, the difference between $A(\vec{k},\omega)$ and corresponding LDA band dispersion is not very obvious. But we believe that when the temperature is low enough and the rotationally invariant interaction is adopted, strong deviations of $A(\vec{k},\omega)$ from LDA band structure can be captured, especially in the low-energy regime. In general, the quasiparticle band structure of cubic phase $BaRuO_3$ coincides with its LDA band structure, giving rise to a picture of moderately correlated metal at ambient condition. On the contrary, previous LDA + DMFT calculations for $CaRuO_3$ and $SrRuO_3$ presented strongly renormalized and shifted quasiparticle band structure,[14] resulting in the picture of strongly correlated metal.

In recent years, the evolutional trend of ferromagnetism in $MRuO_3$ is in hot debate.[5,18,19] Thus in the present works, we calculated the spin-spin correlation function $\chi(\tau)$ and local magnetic susceptibility $\chi_{\rm loc}$ of cubic phase $BaRuO_3$ and tried to elucidate its magnetic properties in finite temperatures. The calculated spin-spin correlation functions are illustrated in Fig. 2(a). On one hand, the cubic phase $BaRuO_3$ exhibits a well-defined frozen local moment, which is characterized by a spin-spin correlation function that approaches nonzero constants at large enough τ, as is easily seen from $T =$ 193–1160 K. On the other hand, the spin-spin correlation function does not behave as $\chi(\tau) \sim [T/\sin(T\tau\pi)]^2$ for times τ sufficiently far from $\tau = 0$ or β, respectively, which means the violation of LFL theory.[35] From the spin-spin correlation function, the local magnetic susceptibility $\chi_{\rm loc} = \int_0^\beta \chi(\tau)d\tau$ can be easily evaluated, which is plotted in Fig. 2(b). As shown, the calculated $\chi_{\rm loc}$ is Curie-Weiss– like over a rather wide temperature range, in other words, it follows a $\chi_{\rm loc}^{-1}(T) = T/C$ law at least up to $T = 1160$ K. This implies that the Ru $4d$ electrons in cubic phase $BaRuO_3$ retain the local nature of the magnetic moment.

Next we concentrate our attentions to the electronic self-energy functions of Ru $4d$ states. The calculated orbital-resolved $\Im\Sigma(i\omega)$ are shown in Fig. 3(a). For the sake of simplicity, only those results calculated at $T = 290$ K are presented. Werner *et al.*[35] have suggested that the still-mysterious optical conductivity $\sigma(\omega)$ in pseudocubic $SrRuO_3$ and $CaRuO_3$, which varies approximately as $\omega^{-0.5}$ and deviates sharply from the prediction of LFL theory, can be perfectly interpreted as a consequence of square-root self-energy function. Inspired by their works, we conducted a careful analysis to determine the asymptotic formula for the low-frequency self-energy function. In a Fermi liquid, the imaginary part of Matsubara self-energy should exhibit a linear regime at low energy, whose slope is directly related to the quasiparticle mass enhancement. However, as shown in Fig. 3(a), we do not observe any linear behavior: the Matsubara self-energy behaves as $-\Im\Sigma(i\omega) = A(i\omega)^\alpha + \gamma$, with $\alpha \sim 0.48$ for t_{2g} states and $\alpha \sim 0.80$ for e_g states, respectively. The nonlinear frequency dependence of the Matsubara self-energy implies that the Landau quasiparticles and effective masses cannot be properly defined for cubic phase $BaRuO_3$, at least at $T = 290$ K. The nonzero intercept $\gamma = -\Im\Sigma(i\omega \to 0)$ can be viewed as the low-energy scattering rate and it is a broadly used physical quantity to distinguish the LFL and non-Fermi-liquid (NFL) phases.[35] As a by-product, the orbital-resolved γ_m is evaluated as a function of temperature and shown in Fig. 3(b). Clearly, γ_m increases monotonously with the increment of

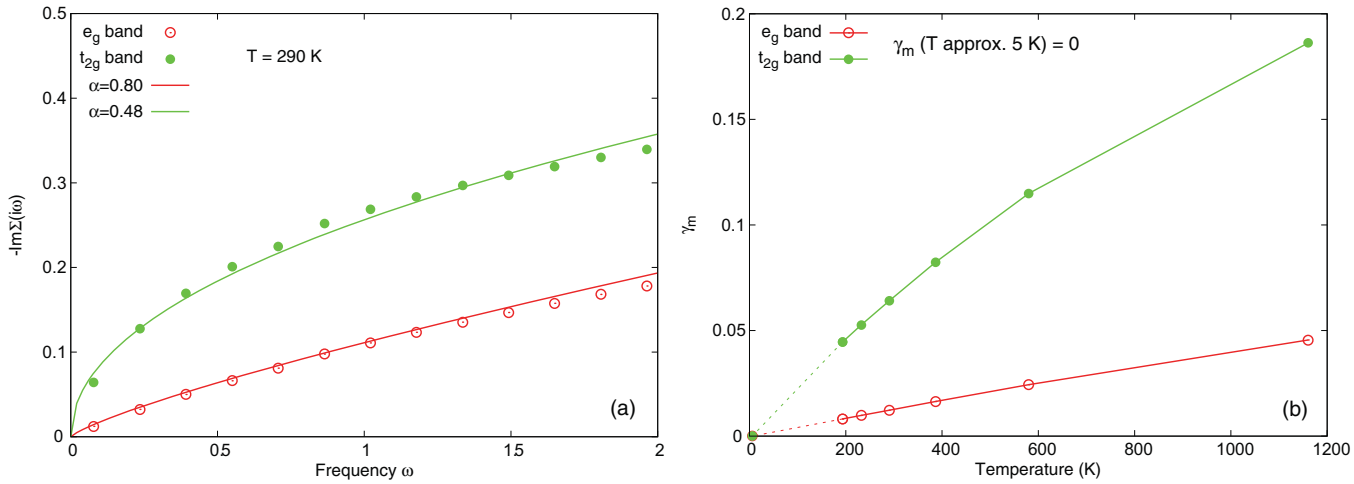

FIG. 3. (Color online) Electronic self-energy function of Ru 4*d* states. (a) Imaginary part of the Matsubara self-energy function $\Im\Sigma(i\omega)$ for t_{2g} and e_g orbitals at $T = 290$ K. The solid lines denote the fitted function $-\Im\Sigma(i\omega) = A(i\omega)^{\alpha} + \gamma$. (b) Orbital-resolved low-energy scattering rate $\gamma_m = -\Im\Sigma_m(i\omega \to 0)$.

temperature and $\gamma_{t_{2g}} > \gamma_{e_g}$ is always valid. For both t_{2g} and e_g states, γ_m cannot be neglected even at $T = 190$ K. We further extrapolate γ_m(T) to zero and obtain the Fermi-liquid temperature $T_{\rm FL} \sim 5$ K. Generally speaking, the restoring of Fermi-liquid behavior only occurs when $T \leqslant T_{\rm FL}$. Thus, it means that similar to $SrRuO_3$ and $CaRuO_3$, at ambient condition the cubic phase $BaRuO_3$ lies in the NFL regime as well.

The most important evidence for NFL state in $SrRuO_3$ and $CaRuO_3$ is the fractional power-law conductivity.[6–8] A power-law analysis on the transport properties, such as resistivity $\rho(T) \propto T^n$, of cubic phase $BaRuO_3$ was made by Zhou *et al.*[19] and the exponent n as a function of pressure was evaluated recently. Their results show an interesting evolution from $n \sim 1.85$, which is close to $n = 2$ for the LFL phase at ambient pressure, to $n \sim 1.4$ of the NFL phase at the pressure where the ferromagnetic phase collapses. However, to our knowledge, the optical conductivity of $BaRuO_3$ has not been investigated by now. In this work, we also calculated the optical conductivity $\sigma(\omega)$ of cubic phase $BaRuO_3$ under various temperatures. As is known, the self-energy function at real axis $\Sigma(\omega)$ is the essential input to calculate the optical conductivity, and the power-law shown in $\Sigma(\omega)$ may be associated with that shown in $\sigma(\omega)$.[35] In order to obtain accurate results, the Legendre polynomial method[29] and improved estimator technique[30] were used to measure the Matsubara self-energy $\Sigma(i\omega)$, and then $\Sigma(i\omega)$ was transformed into $\Sigma(\omega)$ by using the analytical continuation method proposed by Haule *et al.*[33] Finally, the obtained $\Sigma(\omega)$ was cross-checked by the traditional Pade approximation. In Fig. 4 only the real part of optical conductivity is shown. The sharp peak near $\omega = 0$ denotes the Drudelike feature. The broad hump located from 1.5 to 3.5 eV can be attributed to the contribution of electron transition between the quasiparticle peak and Hubbard subbands.[11] With the increment of temperature, this hump shifts slightly to a higher frequency region, which is in accord with the variation trend of Hubbard subbands observed in the temperature-dependent integrated spectral functions of Ru 4*d* states (see Fig. 1). In order to further confirm whether the underlying physics of cubic phase $BaRuO_3$ can be described with LFL theory, we made a detailed power-law analysis for the low-frequency optical conductivity. The low-frequency optical conductivity was fitted by the exponent function $\Re\sigma(\omega) \sim C\omega^{-\alpha}$. The quantitative results are shown in the inset of Fig. 4. The fitted exponent $\alpha \sim 0.98$, while the expected value predicted by LFL theory is $\alpha = 2$. It is worth mentioning that the exponent α is approximately 0.5 for pseudocubic $SrRuO_3$ and $CaRuO_3$, and 0.7 for some high-temperature superconductivity cuprates.[6,7] Nevertheless, the optical conductivity data suggest the NFL metallic nature of cubic phase $BaRuO_3$ under ambient condition again.

Finally, we should emphasize the importance of Hund's physics in cubic phase $BaRuO_3$. Very recent investigations about iron pnictides and chalcogenides showed that strong correlation is not always caused by the Hubbard interaction U but can arise from the Hund's rule coupling J.[36,37] Since the

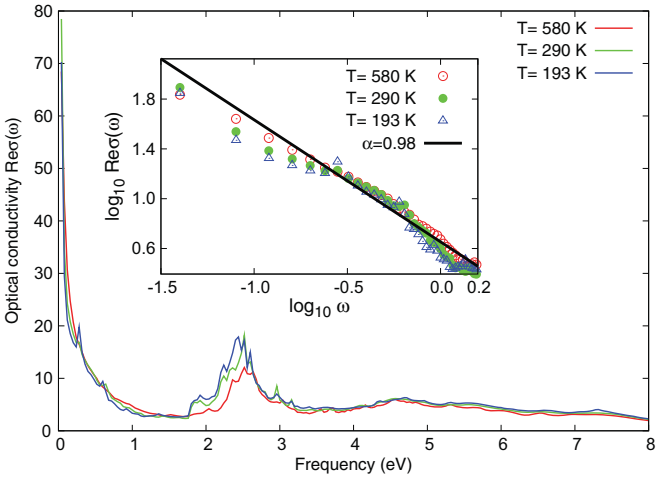

FIG. 4. (Color online) Real part of optical conductivity of cubic perovskite $BaRuO_3$ by LDA + DMFT calculations. Inset: The low-frequency $\Re\sigma(\omega)$ at $T = 193, 290, 580$ K, and the solid bold line represents the fitted function $\Re\sigma(\omega) = C\omega^{-\alpha}$.

strength of electronic correlation in these materials is almost entirely due to the Hund's rule coupling, they are dubbed Hund's metals by Haule and Kotliar[36] at first. It has recently been noticed by Yin *et al*. that in realistic Hund's metals, the electronic self-energy and corresponding optical conductivity show NFL power-law frequency dependence, tendency towards strong orbital differentiation, and that large mass enhancement can occur even though no clear Hubbard subbands exist in the single particle spectra.[34,35,37,38] According to their investigations, both the iron pnictides and chalcogenides are typical Hund's metals. The origin of fractional power law in the optical conductivity of them can be traced to the Hund's rule interaction.[38] As for the cubic phase $BaRuO_3$, based on our calculated results, there is significant NFL behavior and strong orbital differentiation in low-frequency, self-energy function and scattering rate, fractional power law in the optical conductivity, and considerable mass enhancement (at $T = 290$ K, $m^*_{t_{2g}} = 1.8m_0$, and $m^*_{e_g} = 1.2m_0$); thus we can conclude that it is another realistic Hund's metal. Indeed, we have performed additional LDA + DMFT calculations for cubic phase $BaRuO_3$ with different Coulomb interaction strengths from $U = 2.0$ to 6.0 eV and obtained almost identical results. However, when $U = 4.0$ eV and the Hund's rule coupling term is completely ignored ($J = 0.0$ eV), the NFL behaviors previously found in the self-energy function and optical conductivity are absent totally. It should be noted that Medici *et al*.[39,40] have suggested that the physical properties of ruthenates are governed by the Hund's physics, in other words, the pervoskite structure $MRuO_3$ forms a new series of Hund's metal. Our calculated results for the cubic phase $BaRuO_3$ confirm their issue as well.

The type and symmetry of Hund's interaction lead to subtle Hund's physics. When $T < T_{FL}$, the calculated results for density-density and rotationally invariant interactions will be quite different. When the rotationally invariant interaction (both spin-flip and pair-hopping terms are included) is used, we will see a Fermi-liquid ground state. On the contrary, if only the Ising-type (i.e., density-density) interaction is used, the system will stay in the non-Fermi-liquid state. It is proven that the spin-flip terms in the interaction part of the local Hamiltonian are essential in restoring Fermi-liquid behavior at low temperature.[40] When $T > T_{FL}$, the system will show non-Fermi-liquid behavior, and the difference between the Ising-type and fully rotationally invariant Hund's interaction is rather small, or becomes indistinguishable even. Since the T_{FL} for ruthenates may be extremely low (Georges *et al*. conclude that the T_{FL} in typical ruthenates may be below 3 K,[40] and we obtain $T_{FL} \sim 5$ K according to the scattering rate data), in our LDA + DMFT calculations for cubic phase $BaRuO_3$, only the density-density Ising-type interaction is adopted. We believe that because the room temperature is much larger than the Fermi-liquid temperature, the obtained NFL metallic state at ambient condition for cubic phase $BaRuO_3$ is reasonable.

IV. SUMMARY

In summary, to discover a consistent description for the $MRuO_3$-type ruthenates, we study the temperature-dependent physical properties of recently synthesized cubic phase $BaRuO_3$ by using the first-principles LDA + DMFT approach. Judged from the quasiparticle band structure and integrated spectral functions of Ru $4d$ states, the cubic phase $BaRuO_3$ is moderately correlated. There exists local magnetic moment and the inverse local magnetic susceptibility obeys the Curie-Weiss law in the studied temperature regime. The low-frequency self-energy function, scattering rate, and optical conductivity of cubic phase $BaRuO_3$ show apparent NFL behaviors. It is argued that the Hund's rule coupling J plays an important role in the underlying physics in cubic phase $BaRuO_3$ and other perovskite $MRuO_3$ compounds. We believe that the cubic phase $BaRuO_3$ should be another realistic Hund's metal.

ACKNOWLEDGMENTS

L.H. was supported by the National Science Foundation of China and received support from the 973 Program of China under Contracts No. 2007CB925000 and No. 2011CBA00108. B.Y.A. was supported by the National Science Foundation of China under Contract No. 20971114.

[1] Y. Maeno, H. Hashimoto, K. Yoshida, S. Nishizaki, T. Fujita, J. G. Bednorz, and F. Lichtenberg, Nature (London) **372**, 532 (1994).
[2] S. Nakatsuji and Y. Maeno, Phys. Rev. Lett. **84**, 2666 (2000).
[3] V. I. Anisimov, I. A. Nekrasov, D. E. Kondakov, T. M. Rice, and M. Sigrist, Eur. Phys. J. B **25**, 191 (2002).
[4] G. Koster, L. Klein, W. Siemons, G. Rijnders, J. S. Dodge, C.-B. Eom, D. H. A. Blank, and M. R. Beasley, Rev. Mod. Phys. **84**, 253 (2012).
[5] G. Cao, S. McCall, M. Shepard, J. E. Crow, and R. P. Guertin, Phys. Rev. B **56**, 321 (1997).
[6] P. Kostic, Y. Okada, N. C. Collins, Z. Schlesinger, J. W. Reiner, L. Klein, A. Kapitulnik, T. H. Geballe, and M. R. Beasley, Phys. Rev. Lett. **81**, 2498 (1998).
[7] J. S. Dodge, C. P. Weber, J. Corson, J. Orenstein, Z. Schlesinger, J. W. Reiner, and M. R. Beasley, Phys. Rev. Lett. **85**, 4932 (2000).
[8] Y. S. Lee, J. Yu, J. S. Lee, T. W. Noh, T.-H. Gimm, H.-Y. Choi, and C. B. Eom, Phys. Rev. B **66**, 041104 (2002).
[9] M. S. Laad, I. Bradarić, and F. V. Kusmartsev, Phys. Rev. Lett. **100**, 096402 (2008).
[10] M. Takizawa, D. Toyota, H. Wadati, A. Chikamatsu, H. Kumigashira, A. Fujimori, M. Oshima, Z. Fang, M. Lippmaa, M. Kawasaki, and H. Koinuma, Phys. Rev. B **72**, 060404 (2005).
[11] J. S. Ahn, J. Bak, H. S. Choi, T. W. Noh, J. E. Han, Y. Bang, J. H. Cho, and Q. X. Jia, Phys. Rev. Lett. **82**, 5321 (1999).
[12] K. Maiti and R. S. Singh, Phys. Rev. B **71**, 161102 (2005).
[13] K. Maiti, Phys. Rev. B **73**, 235110 (2006).
[14] E. Jakobi, S. Kanungo, S. Sarkar, S. Schmitt, and T. Saha-Dasgupta, Phys. Rev. B **83**, 041103 (2011).
[15] H. Hadipour and M. Akhavan, Eur. Phys. J. B **84**, 203 (2011).

[16] Y. S. Lee, T. W. Noh, J. H. Park, K.-B. Lee, G. Cao, J. E. Crow, M. K. Lee, C. B. Eom, E. J. Oh, and I.-S. Yang, Phys. Rev. B **65**, 235113 (2002).
[17] C. Felser and R. J. Cava, Phys. Rev. B **61**, 10005 (2000).
[18] C.-Q. Jin, J.-S. Zhou, J. B. Goodenough, Q. Q. Liu, J. G. Zhao, L. X. Yang, Y. Yu, R. C. Yu, T. Katsura, A. Shatskiy, and E. Ito, Proc. Nat. Acad. Sci. **105**, 7115 (2008).
[19] J.-S. Zhou, K. Matsubayashi, Y. Uwatoko, C.-Q. Jin, J.-G. Cheng, J. B. Goodenough, Q. Q. Liu, T. Katsura, A. Shatskiy, and E. Ito, Phys. Rev. Lett. **101**, 077206 (2008).
[20] A. Georges, G. Kotliar, W. Krauth, and M. J. Rozenberg, Rev. Mod. Phys. **68**, 13 (1996).
[21] G. Kotliar, S. Y. Savrasov, K. Haule, V. S. Oudovenko, O. Parcollet, and C. A. Marianetti, Rev. Mod. Phys. **78**, 865 (2006).
[22] B. Amadon, F. Lechermann, A. Georges, F. Jollet, T. O. Wehling, and A. I. Lichtenstein, Phys. Rev. B **77**, 205112 (2008).
[23] P. Giannozzi, S. Baroni, N. Bonini, M. Calandra, R. Car, C. Cavazzoni, D. Ceresoli, G. L. Chiarotti, M. Cococcioni, I. Dabo, A. Dal Corso, S. de Gironcoli, S. Fabris, G. Fratesi, R. Gebauer, U. Gerstmann, C. Gougoussis, A. Kokalj, M. Lazzeri, L. Martin-Samos *et al.*, J. Phys.: Condens. Matter **21**, 395502 (2009).
[24] J. P. Perdew, K. Burke, and M. Ernzerhof, Phys. Rev. Lett. **77**, 3865 (1996).
[25] P. E. Blöchl, Phys. Rev. B **50**, 17953 (1994).
[26] B. Amadon, F. Jollet, and M. Torrent, Phys. Rev. B **77**, 155104 (2008).
[27] P. Werner, A. Comanac, L. de' Medici, M. Troyer, and A. J. Millis, Phys. Rev. Lett. **97**, 076405 (2006).
[28] E. Gull, A. J. Millis, A. I. Lichtenstein, A. N. Rubtsov, M. Troyer, and P. Werner, Rev. Mod. Phys. **83**, 349 (2011).
[29] L. Boehnke, H. Hafermann, M. Ferrero, F. Lechermann, and O. Parcollet, Phys. Rev. B **84**, 075145 (2011).
[30] H. Hafermann, K. R. Patton, and P. Werner, Phys. Rev. B **85**, 205106 (2012).
[31] M. Jarrell and J. Gubernatis, Phys. Rep. **269**, 133 (1996).
[32] K. S. D. Beach, arXiv:cond-mat/0403055.
[33] K. Haule, C.-H. Yee, and K. Kim, Phys. Rev. B **81**, 195107 (2010).
[34] A. Kutepov, K. Haule, S. Y. Savrasov, and G. Kotliar, Phys. Rev. B **82**, 045105 (2010).
[35] P. Werner, E. Gull, M. Troyer, and A. J. Millis, Phys. Rev. Lett. **101**, 166405 (2008).
[36] K. Haule and G. Kotliar, New J. Phys. **11**, 025021 (2009).
[37] Z. P. Yin, K. Haule, and G. Kotliar, Nat. Mater. **10**, 932 (2011).
[38] Z. P. Yin, K. Haule, and G. Kotliar, Phys. Rev. B **86**, 195141 (2012).
[39] L. de' Medici, J. Mravlje, and A. Georges, Phys. Rev. Lett. **107**, 256401 (2011).
[40] A. Georges, L. de' Medici, and J. Mravlje, Annu. Rev. Condens. Matter Phys. **4**, 137 (2013).